Operational Reliability Model of Hybrid MMC Considering Multiple Time Scales and Multi-state Submodule

Fei Feng, Juan Yu, Wei Dai, Zhifang Yang, Xingpan Zhao, Salah Kamel, and Guobin Fu

***Abstract*—Environmental and electrical factors such as wind speed, air temperature and switching frequency have significant influences on the operational reliability of hybrid modular multilevel converter (MMC), which is commonly used for the wind power transmission. However, the existing reliability model of hybrid MMC based on statistics cannot accurately reflect the impact of these factors. In this paper, a new operational reliability model of hybrid MMC is presented. The reliability index of the hybrid MMC is coupled with its operation characteristics by calculating multi-term thermal cycling. In addition, an operation strategy of hybrid MMC is proposed to improve its reliability. The multi-state submodule (SM) is developed, which is capable of bypassing specific faulty power modules instead of the whole SM. Case studies show that the proposed operational reliability model could describe the impact of environmental and electrical factors. Also, the proposed operation strategy can improve the reliability of hybrid MMC by extending the operation time of SMs.**

***Index Terms*—Modular multilevel converter (MMC), multiple time scales, submodule (SM), operational reliability, thermal cycling.**

I. INTRODUCTION

MODULAR multilevel converter based high voltage direct current (MMC-HVDC) transmission is a promising technology for large-scale wind power integration because of the low distortion of output voltage and decoupling control of active and reactive power [1]-[3]. As a key component in MMC-HVDC system, the operational reliability of MMC is significant for the stable operation of the system. In fact, failure rates of MMC components are closely related to environmental and electrical factors. The main influencing factors include wind speed, air temperature and switching frequency. The output power of MMC for wind power transmission greatly changes with the wind speed fluctuation [4], [5]. It will affect the junction temperature swings of power devices, and eventually influence the reliability of MMC. The thermal cycles will fluctuate with the variation of air temperature, thereby seriously affecting the operational reliability of MMC [6]. In addition, as the installed wind power capacity increases, more MMC components need to be used to fulfill the higher voltage requirement. The impact of installed electrical parameters on the operational reliability of MMC could not be ignored such as switching frequency and current alternating [7]. However, solely statistical reliability evaluation may distort the impact of current working conditions, causing significant deviation of reliability model from reality [8]. Therefore, an operational reliability model of MMC that accurately measures the impact of multiple factors becomes quite meaningful in the wind power transmission system.

Because of its good DC fault ride-through capability and economical investment, hybrid MMC is an attractive technology in industrial applications [9], [10]. Therefore, many types of submodules (SMs) with DC fault ride-through capability have been developed. Because of similar function, they can substitute each other in some circumstances [11]. However, in the conventional operation strategy of hybrid MMC, the operating SM has been bypassed whenever any device in the SM fails [12]. This would limit the operation time of SMs, thereby affecting the reliability of hybrid MMC. It becomes quite meaningful to improve the operation strategy to improve the reliability of hybrid MMC.

Facing these problems, an operational reliability model of hybrid MMC is developed with consideration of environmental and electrical factors. Based on this model, an improved operation strategy is proposed to improve the reliability of hybrid MMC.

Existing studies on the reliability of MMC mainly include equipment and component levels. For reliability of MMC at the equipment level, recently, many reliability models of MMC have been proposed [11]-[19]. In [11], [13], different initial redundant methods of SMs are proposed to get the optimal trade-off between SM cost and reliability for MMC.

Manuscript received: April 4, 2019; accepted: January 13, 2020. Date of CrossCheck: January 13, 2020. Date of online publication: September 1, 2020.

This work was supported by the National Key R&D Program of China (No. 2017YFB0902200), the Science and Technology Project of State Grid Corporation of China (No. 5228001700CW), and the International Cooperation and Exchange Project of National Natural Science Foundation of China (No. 51861145406).

F. Feng, J. Yu (corresponding author), W. Dai, Z. Yang, and S. Kamel are with State Key Laboratory of Power Transmission Equipment & System Security and New Technology, Chongqing University, Chongqing 400044, China (e-mail: fengfeiduan@foxmail. com; 148454745@qq. com; 1209340673@qq. com; yangzfang@126.com; skamel@aswu.edu.eg).

X. Zhao is with Chuxiong Power Supply Bureau of Yunnan Power Grid, Chuxiong 67500, China (e-mail: 2465185700@qq.com).

G. Fu is with Electric Power Research Institute, State Grid Qinghai Electric Power Company, Xining 810008, China (e-mail: 421102468@qq.com).

DOI: 10.35833/MPCE.2019.000227

The impacts of preventive periodic maintenance, different redundancy and different topologies and packages of SMs on the reliability of MMC are taken into account [12], [14]-[16]. Correlations between the requisite and redundant SMs are considered in hybrid MMC and usual MMC, respectively [17]-[19]. However, the reliability models of MMC are mainly established based on the statistical failure rate. In fact, the failure rates of power devices are time-varying and the influence comes from multiple factors [20], [21], which indicates that the assumption of constant rate still can be improved.

For reliability of MMC at the component level, the failure mechanisms of power devices in wind power system are related with many factors such as thermal cycling, blocking voltage and power-on-time [22], [23]. The thermal cycling is considered as one of the most critical failure reasons. Furthermore, thermal cycles with long-term time scale are mainly influenced by wind speed and ambient temperature, while the thermal cycles with the short-term time scale are mainly affected by electrical factors, e.g., power current alternating. Both of them can affect the lifetime of power devices [24], [25]. References [6], [7] evaluate the lifetime of power devices in half-bridge MMC based on physics of reliability and Miner's rule [26], which can be used for redundancy design. Also, it has demonstrated that power devices bear serious thermal stress because of the fluctuation of wind speed. However, the reliability of power devices in hybrid MMC is not investigated.

In conventional operation strategy of hybrid MMC, the operating SM will be bypassed when any power device in the SM fails [12]. However, in fact, when some specific power devices fail, some types of SMs can still be used to support the DC-link voltage by bypassing these power modules such as unipolar-voltage full-bridge SM (UFSM) [27] and self-blocked SM (SBSM) [28]. It may help to extend the working time of SM and improve the reliability of hybrid MMC.

This paper investigates the reliability model and the operation strategy of hybrid MMC, which contains the following three main contributions.

1) The reliability of power components in hybrid MMC considering environmental and electrical factors is analyzed based on thermal cycling with multiple time scales. Thermal cycles are calculated by using the foster model and operation characteristics of hybrid MMC.

2) A new operation strategy of hybrid MMC with multi-state SM is proposed to improve the reliability. The operation strategy is improved by bypassing specific faulty component instead of the whole SM based on the operation principle of SM. The corresponding reliability model is derived based on the multinomial distribution.

3) An operational reliability model of hybrid MMC with multiple time scales and multi-state SM is proposed based on reliability of components with multiple time scales, improved SM operation strategy and structure of hybrid MMC. The proposed model is capable of accurately measuring the impact of different factors on hybrid MMC reliability.

II. Operation Characteristics of Hybrid MMC in Wind Power Transmission System

This section introduces the operation characteristics and structure of hybrid MMC, which is the basis of analysis on operational reliability of hybrid MMC.

Figure 1 shows the topology of a three-phase hybrid MMC. Each arm is composed of series-connected SMs. SMs consist of insulated gate bipolar transistor (IGBTs), diodes and capacitors. In the topology of hybrid MMC, the half-bridge SM (HBSM) supports the DC-link voltage, and other SMs are installed for both supporting the DC-link voltage and DC fault ride-through. In this paper, the hybrid MMC topology consists of N_{HBs} HBSMs and N_{UFs} UFSMs. In addition, an active redundancy scheme is used in this paper, which is normally used in the actual industrial MMC-HVDC projects.

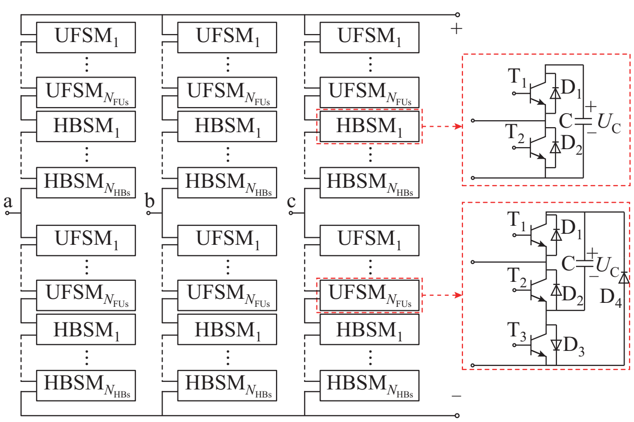

Fig. 1. Topology of a three-phase hybrid MMC.

In the wind power transmission system, the active power of hybrid MMC P_{MMCout} equals to the sum of output power of wind turbine generators (WTGs). The relationship between the i^{th} WTG output power $P_{\mathrm{WTGout},\,i}$ and wind speed V_{t_n} at current time point t_n, where n is the number of time point samples, can be expressed as [29]:

$$P_{\mathrm{WTGout},i}=\begin{cases}0 & 0<V_{t_n}<V_{\mathrm{cut\text{-}in}}\\ k_{\mathrm{p}}V_{t_n}^3 & V_{\mathrm{cut\text{-}in}}\leq V_{t_n}<V_{\mathrm{rated}}\\ P_{\mathrm{rated}} & V_{\mathrm{rated}}\leq V_{t_n}<V_{\mathrm{cut\text{-}out}}\\ 0 & V_{\mathrm{cut\text{-}out}}\leq V_{t_n}\end{cases}\tag{1}$$

where $V_{\mathrm{cut\text{-}in}}$, V_{rated}, and $V_{\mathrm{cut\text{-}out}}$ are the cut-in, rated, and cut-out wind speeds, respectively; P_{rated} is the rated capacity of WTG; and k_{p} is a constant related to the density of air and blade area of WTG.

Given that the arm current operates normally without harmonic circulating current, the up and down arm currents can be expressed as, respectively [9]:

$$\begin{cases}i_{\mathrm{au}}=\dfrac{I_{\mathrm{dc}}}{3}+\dfrac{I_{\mathrm{m}}}{2}\sin(2\pi f_0t-\varphi)\\ i_{\mathrm{ad}}=\dfrac{I_{\mathrm{dc}}}{3}-\dfrac{I_{\mathrm{m}}}{2}\sin(2\pi f_0t-\varphi)\end{cases}\tag{2}$$

where φ is the voltage or current phase angle; f_0 is the fundamental frequency; I_m and I_{dc} are the peak AC output phase current and the DC current, respectively, which can be approximated as:

$$\begin{cases} I_m \approx \dfrac{2P_{\text{MMCout}}}{3U_m \cos\varphi} \\ I_{dc} \approx \dfrac{P_{\text{MMCout}}}{U_{dc}} \end{cases} \tag{3}$$

where U_m and U_{dc} are the peak AC output voltage and the DC voltage, respectively.

The operation scheme of the UFSM and HBSM, e.g., the SM voltage U_{SM} and the switch state S_{TATE}, are shown in Table I. In the normal operation, the power module containing IGBT T_3 and diode D_3 is always turned on, which is equivalent to a short circuit. The diode D_4 is turned off all the time and equivalent to an open circuit. Therefore, UFSM is equivalent to HBSM in the normal working state.

TABLE I
OPERATION SCHEME OF SMS

SM	S_{TATE}	T_1	T_2	T_3	U_{SM}
UFSM	1	Off	On	On	0
	2	On	Off	On	U_C
	Block	Off	Off	Off	-
HBSM	1	Off	On	-	0
	2	On	Off	-	U_C

Note: "-" means the index does not exist.

A sinusoidal pulse width modulation (SPWM) scheme is applied to control the switch of IGBTs. During the working procedure of IGBTs, conduction loss and switching loss are usually considered. We assume that a fundamental frequency cycle contains n_{sw} switching cycles ($n_{sw}=f_{sw}/f_0$). For IGBT, the average power loss $P_{T,avg}^{(j)}$ at the j^{th} switching cycles ($j=1,2,\ldots,n_{sw}$) is the sum of conduction loss $P_{T,con}^{(j)}$ and switching loss $P_{T,sw}^{(j)}$, which can be calculated as [30], [31]:

$$P_{T,avg}^{(j)} = P_{T,con}^{(j)} + P_{T,sw}^{(j)} = (R_{ce} i_{au} + U_{ceo} i_{au})\tau_T + (a_T i_{au}^3 + b_T i_{au}^2 + c_T i_{au}) \frac{U_d}{U_{\text{rated}}} f_{sw} \rho_T \tag{4}$$

where R_{ce} and U_{ceo} are the forward conduction resistance, and the voltage drop on IGBT, respectively; f_{sw} is the switching frequency; a_T, b_T, and c_T are the curve fitting parameters; ρ_T is the coefficient related to the junction temperature; U_{rated} is the reference voltage of IGBT; U_d is the DC voltage of IGBT; and τ_T is the duty cycles. The diode could be calculated by using similar approach for average power loss.

From (1) to (4), it can be obtained that the electrical parameters of WTG and wind speed influence the arm current of hybrid MMC, which affects the power loss of semiconductors. Meanwhile, the electrical parameters of hybrid MMC affect the power loss of semiconductors directly.

III. RELIABILITY MODELING OF POWER COMPONENTS IN HYBRID MMC WITH MULTIPLE TIME SCALES

To analyze the reliability difference among components in hybrid MMC and evaluate the impact of environmental and electrical factors on hybrid MMC, this paper presents a reliability model to describe the operation characteristics of hybrid MMC.

A. Thermal Cycling with Multiple Time Scales

The junction temperature of power devices in hybrid MMC varies with the power loss during the operation process. The thermal equivalent circuits can be used to obtain the junction temperature of power devices, which can be obtained by using the foster model [32].

According to the manufacturer datasheet given in [33], the thermal network from the junction to the case can be constructed by a fourth-order foster model. The thermal network from the case to heat sink and the thermal network from heat sink to ambient are established by first-order foster models, respectively. Based on the foster model, the junction temperature of IGBT at the j^{th} switching cycle can be calculated as [33]:

$$T_{Tj}^{(j)} = \sum_{i=1}^{4} \Delta T_{Tjc,i}^{(j)} + \Delta T_{Tch}^{(j)} + \Delta T_{ha}^{(j)} + T_{a,t_n} \tag{5}$$

where T_{a,t_n} is the ambient temperature at sample time t_n; $\Delta T_{Tjc,i}^{(j)}$ is the switching cycle temperature junction difference (SCTD) of the i^{th} RC parallel unit in IGBT junction to the case thermal network; $\Delta T_{Tch}^{(j)}$ is SCTD of IGBT case to heat sink; and $\Delta T_{ha}^{(j)}$ is the SCTD of heat sink to ambient.

The SCTD $\Delta T_{Tjc,i}^{(j)}$ can be expressed as:

$$\Delta T_{Tjc,i}^{(j)} = P_{T,avg}^{(j)} R_{Tjc,i} \left(1 - e^{\frac{-T_{sw}}{\tau_{Tjc,i}}}\right) + \Delta T_{Tjc,i}^{(j-1)} e^{\frac{-T_{sw}}{\tau_{Tjc,i}}} \tag{6}$$

where $R_{Tjc,i}$ and $\tau_{Tjc,i}$ are the thermal resistance and time constant of the i^{th} IGBT junction to the case thermal network, respectively; T_{sw} is the switching period; and $\Delta T_{Tjc,i}^{(j-1)}$ is the SCTD at the $(j-1)^{th}$ switching cycle. Other $\Delta T_{Tjc,i}^{(j)}$ shares the similar formulation. For $\Delta T_{Tch}^{(j)}$ and $\Delta T_{ha}^{(j)}$, because the change of the case temperature is slower, they can be approximated as a constant in a fundamental cycle [29].

In general, the changes of electrical factors such as the current and duty cycle can be reflected in thermal cycles with short-term time scale because of the small time constant (second-level) as shown in Fig. 2.

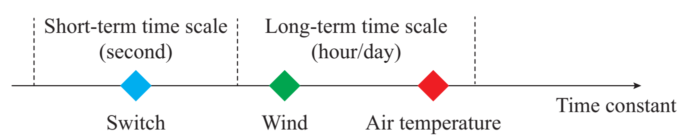

Fig. 2. Variations of different factors with different time scales.

In the operation process, the sample data of wind speed and ambient temperature is extracted at every time interval T. Each time interval T consists of $N_{T,F}$ fundamental frequency cycles ($N_{T,F}=Tf_0$). According to (5) and (6), all of the switching cycle junction temperatures in the i^{th} fundamental frequency cycle ($i=1,2,\ldots,N_{T,F}$) are calculated by iterating SCTDs. Then, the mean junction temperature $T_{Tjavg,F}$, maximum value $T_{\mathrm{Tjmax,F}}$, minimum value $T_{\mathrm{Tjmin,F}}$, current of wire bond and the chip I_{F} per fundamental frequency thermal cycle can be obtained.

The impact of wind speed and ambient temperature that have large time constant (e.g., hour, day) can be reflected in low-frequency thermal cycles with long-term time scale. Because of the fluctuation of the wind speed and ambient temperature, the junction temperature is usually randomly ordered. The rain flow counting method [34] can be used to extract thermal parameters from disordered thermal cycles for fatigue lifetime estimation. Based on the rain flow counting method, $N_{\mathrm{Tsum,L}}$ low frequency thermal cycles can be obtained by using the mean junction temperature $T_{\mathrm{Tjavg,F}}$ from t_0 to the sample time t_n. Then, the maximum junction temperature $T_{\mathrm{Tjmax,L}}$, minimum junction temperature $T_{\mathrm{Tjmin,L}}$, current of wire bond and the chip I_{L} per low frequency thermal cycle can be calculated.

The parameter calculation of the diode can be executed by using the similar approach.

B. Reliability of Power Devices in Hybrid MMC with Multiple Time Scales

Based on the long-term and short-term thermal cycles considering the impacts of multi-factors, Bayerer model can be used to evaluate the consumed lifetime of power devices [23].

To evaluate the impact of low frequency thermal cycles on IGBT, the number of cycles to failure $N_{\mathrm{Tf,L}}$ can be calculated by using $T_{\mathrm{Tjmax,L}}$, $T_{\mathrm{Tjmin,L}}$ and I_{L} per low frequency thermal cycle based on Bayerer model [23]:

$$N_{\mathrm{Tf,L}}=k(T_{\mathrm{Tjmax,L}}-T_{\mathrm{Tjmin,L}})^{\beta_1}\mathrm{e}^{\frac{\beta_2}{T_{\mathrm{Tjmin,L}}+273}}t_{\mathrm{on}}^{\beta_3}I_{\mathrm{L}}^{\beta_4}U^{\beta_5}D^{\beta_6} \tag{7}$$

where t_{on} is the time dependence; U is the blocking voltage; D is the diameter of the bonding wire; $k=9.3\times10^{14}$; $\beta_1=-4.416$; $\beta_2=1285$; $\beta_3=-0.463$; $\beta_4=-0.716$; $\beta_5=-0.761$; and $\beta_6=-0.5$.

To estimate the influence of fundamental frequency thermal cycles, the number of cycles to failure $N_{\mathrm{Tf,F}}$ can be calculated in a similar way.

For IGBT, the total consumed lifetime with multiple time scales during t_0-t_n $CL_{\mathrm{T}}(t_n)$ and the mean time to failure at t_n $MTTF_{\mathrm{T}}(t_n)$ can be accumulated based on Miner's rule [26], [35], which are expressed as:

$$CL_{\mathrm{T}}(t_n)=\sum_{i=1}^{N_{\mathrm{Tsum,L}}}\frac{N_{\mathrm{T,L},i}}{N_{\mathrm{Tf,L},i}}+\sum_{i=1}^{n}\frac{N_{\mathrm{T,F},i}}{N_{\mathrm{Tf,F},i}} \tag{8}$$

$$MTTF_{\mathrm{T}}(t_n)=\frac{T}{\int_{t_{n-1}}^{t_n}CL_{\mathrm{T}}(t)\mathrm{d}t} \tag{9}$$

where $N_{\mathrm{T,L},i}$ and $N_{\mathrm{Tf,L},i}$ are the number of cycles and the number of cycles to failure of the i^{th} low frequency thermal cycle, respectively; and $N_{\mathrm{T,F},i}$ and $N_{\mathrm{Tf,F},i}$ are the number of cycles and the number of cycles to the failure of the fundamental frequency thermal cycle during the i^{th} sampling interval, respectively.

According to the definition of the failure rate of power devices [36], the failure rate of IGBT $\lambda_{\mathrm{T}}(t_n)$ can be expressed as:

$$\lambda_{\mathrm{T}}(t_n)=\frac{1}{MTTF_{\mathrm{T}}(t_n)} \tag{10}$$

The reliability indices of diode, e.g., the consumed lifetime $CL_{\mathrm{D}}(t_n)$, the mean time to failure $MTTF_{\mathrm{D}}(t_n)$ and the failure rate $\lambda_{\mathrm{D}}(t_n)$, can be obtained by using the similar procedure.

IV. Operational Reliability Model of Hybrid MMC with Multi-state SM

In this section, an operational reliability model of hybrid MMC with multi-state SM is proposed with consideration of a new SM operation strategy, based on the reliability of power devices with multiple time scales and the structure of hybrid MMC.

A. Operation Strategy with Multi-state SM

UFSM works for supporting both the DC-link voltage and DC fault ride-through. Assuming the input direction is positive in Fig. 3, in normal states, if the current is positive, the current will go through D_3. If the current is negative, the current will go through T_3. Therefore, the power module containing T_3 and D_3 is always turned on, which is equivalent to a short circuit. Meanwhile, the diode D_4 is turned off all the time and equivalent to an open circuit. In the conventional SM operation strategy, UFSM will be bypassed when either T_3 or D_3 fails. In fact, when T_3 or D_3 fails, UFSM can still operate like HBSM to support the DC-link voltage by bypassing the faulty part with auxiliary settings. Therefore, the difference from tradition strategy is that module T_3 fails, it will be bypassed, while other modules in UFSM can go on working. As shown in Fig. 3(b), the UFSM can turn into a single function state as HBSM to support the DC-link voltage by the short circuit of faulty module T_3. Other power modules do not need to change operation principle. In other words, the UFSM with single function state can be equivalent to HBSM to support the DC-link voltage. The operation scheme of single-function UFSM is the same as the operation scheme of HBSM.

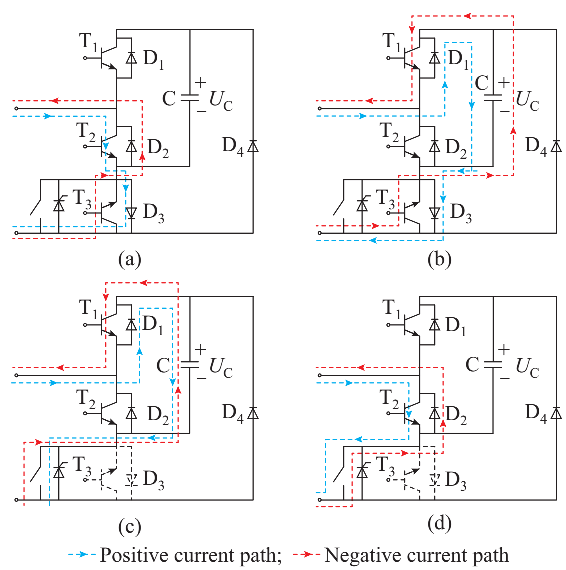

Fig. 3. Status of multi-state UFSM. (a) Normal state 1. (b) Normal state 2. (c) Single function state 1. (d) Single function state 2.

B. Reliability Model of Multi-state SM

For IGBT and diode, the failure rate is time-variant with the operation conditions. The reliability functions of IGBT and diode can be represented as:

$$R_{\mathrm{T}x}(t_n)=\mathrm{e}^{-\int_0^{t_n}\lambda_{\mathrm{T}}(t)\mathrm{d}t} \tag{11}$$

$$R_{\mathrm{D}x}(t_n)=\mathrm{e}^{-\int_0^{t_n}\lambda_{\mathrm{D}}(t)\mathrm{d}t} \tag{12}$$

where $x=1,2,3$.

Metallized-film capacitors are widely used in MMCs because of the characteristics of self-healing. However, in the active scheme, normal SMs share the voltage of faulty SMs which affect the reliability of SMs. Therefore, a voltage factor is used for the reliability of capacitor $R_{\mathrm{C}}(t_n)$ to represent the impact of self-healing energy as [12], [37]:

$$R_{\mathrm{C}}(t_n)=\mathrm{e}^{-\lambda_{\mathrm{C}_0}\upsilon_s^{\eta}t_n} \tag{13}$$

where λ_{C_0} is the failure rate of capacitor; υ_{s} is the ratio of the applied voltage with respect to the nominal voltage; and η is the voltage stress factor, which varies with component types [37].

In the normal UFSM, HBSM, IGBT, diode and capacitor are connected in series, as shown in Fig. 3(a), (b). The reliability of these auxiliary setting in this paper is considered to have zero failure rate since the bypass switches operate in exceptional circumstances. Hence, the reliability of UFSM and HBSM $R_{\mathrm{UFn}}(t_n)$ and $R_{\mathrm{HBn}}(t_n)$ can be represented as:

$$R_{\mathrm{UFn}}(t_n)=R_{\mathrm{T1}}(t_n)R_{\mathrm{D1}}(t_n)R_{\mathrm{T2}}(t_n)R_{\mathrm{D2}}(t_n)R_{\mathrm{T3}}(t_n)R_{\mathrm{D3}}(t_n)R_{\mathrm{C}}(t_n) \tag{14}$$

$$R_{\mathrm{HBn}}(t_n)=R_{\mathrm{T1}}(t_n)R_{\mathrm{D1}}(t_n)R_{\mathrm{T2}}(t_n)R_{\mathrm{D2}}(t_n)R_{\mathrm{C}}(t_n) \tag{15}$$

Similarly, the reliability of single-function UFSM $R_{\mathrm{UFp}}(t_n)$ can be expressed as:

$$R_{\mathrm{UFp}}(t_n)=R_{\mathrm{T1}}(t_n)R_{\mathrm{D1}}(t_n)R_{\mathrm{T2}}(t_n)R_{\mathrm{D2}}(t_n)(1-R_{\mathrm{T3}}(t_n)R_{\mathrm{D3}}(t_n))\,R_{\mathrm{C}}(t_n) \tag{16}$$

C. Operational Reliability Model of Hybrid MMC with Multi-state SM

According to the topology of hybrid MMC, UFSMs and HBSMs are connected in series at one arm. When the number of faulty HBSMs is more than that of redundant HBSMs, both normal and single-function UFSMs can be used to substitute faulty HBSMs. Hence, the hybrid MMC can be operated as Fig. 4.

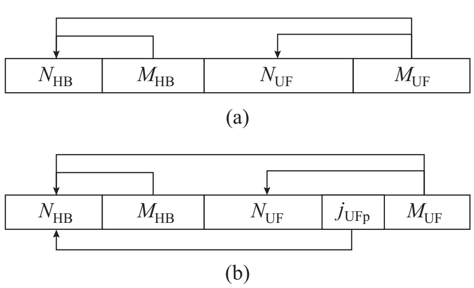

Fig. 4. Substitution relationship of SMs in hybrid MMC with multi-state SM. (a) Operation state 1. (b) Operation state 2.

1) In the operation state 1, the number of the faulty UFSM and HBSM is not more than the redundant amount, i.e., $j_{\mathrm{UF}}\le M_{\mathrm{UF}}$, $j_{\mathrm{HB}}\le M_{\mathrm{HB}}$, then, the hybrid MMC can operate normally.

Based on the binomial distribution formula and the series-connected structure of UFSMs [14], the reliability of UFSMs $R_{\mathrm{UFs1}}(t_n)$ can be given as:

$$R_{\mathrm{UFs1}}(t_n)=\sum_{j_{\mathrm{UF}}=0}^{M_{\mathrm{UF}}}\frac{(N_{\mathrm{UF}}+M_{\mathrm{UF}})!}{j_{\mathrm{UF}}!}(R_{\mathrm{UFn}}(t_n))^{N_{\mathrm{UF}}+M_{\mathrm{UF}}-j_{\mathrm{UF}}}(1-R_{\mathrm{UFn}}(t_n))^{j_{\mathrm{UF}}} \tag{17}$$

where N_{UF} is the requisite number of UFSM.

Similarly, the reliability of HBSMs $R_{\mathrm{HBs1}}(t_n)$ can be given as:

$$R_{\mathrm{HBs1}}(t_n)=\sum_{j_{\mathrm{HB}}=0}^{M_{\mathrm{HB}}}\frac{(N_{\mathrm{HB}}+M_{\mathrm{HB}})!}{j_{\mathrm{HB}}!}(R_{\mathrm{HBn}}(t_n))^{N_{\mathrm{HB}}+M_{\mathrm{HB}}-j_{\mathrm{HB}}}(1-R_{\mathrm{HBn}}(t_n))^{j_{\mathrm{HB}}} \tag{18}$$

where N_{HB} is the requisite number of HBSM.

Based on the series-connected structure of UFSMs and HBSMs, the reliability of arm $R_{\mathrm{Arm,u1}}(t_n)$ can be given as:

$$R_{\mathrm{Arm,u1}}(t_n)=R_{\mathrm{UFs1}}(t_n)R_{\mathrm{HBs1}}(t_n) \tag{19}$$

2) In the operation state 2, the number of faulty HBSM is over redundancy. To keep hybrid MMC operating normally, the normal UFSMs and single-function UFSMs need to substitute faulty HBSMs. Meanwhile, the faulty number of UFSM should not surpass UFSM redundancy. Therefore, the faulty HBSMs should satisfy $M_{\mathrm{HB}}<j_{\mathrm{HB}}\le M_{\mathrm{HB}}+M_{\mathrm{UF}}-j_{\mathrm{UF}}+j_{\mathrm{UFp}}$. Besides, the faulty UFSMs should satisfy $j_{\mathrm{UF}}\le M_{\mathrm{UF}}$.

Based on the multinomial distribution formula and the series-connected structure of UFSMs, the reliability of UFSMs $R_{\mathrm{UFs2}}(t_n)$ can be given as:

$$\begin{aligned}R_{\mathrm{UFs2}}(t_n)=&\sum_{j_{\mathrm{UF}}=0}^{M_{\mathrm{UF}}}\sum_{j_{\mathrm{UFp}}=0}^{j_{\mathrm{UF}}}\frac{(N_{\mathrm{UF}}+M_{\mathrm{UF}})!}{(N_{\mathrm{UF}}+M_{\mathrm{UF}}-j_{\mathrm{UF}})!j_{\mathrm{UFp}}!(j_{\mathrm{UF}}-j_{\mathrm{UFp}})!}\cdot\\&(R_{\mathrm{UFn}}(t_n))^{N_{\mathrm{UF}}+M_{\mathrm{UF}}-j_{\mathrm{UF}}}(R_{\mathrm{UFp}}(t_n))^{j_{\mathrm{UFp}}}(1-R_{\mathrm{UFn}}(t_n)-\\&R_{\mathrm{UFp}}(t_n))^{j_{\mathrm{UF}}-j_{\mathrm{UFp}}}\end{aligned} \tag{20}$$

The reliability of HBSMs $R_{\mathrm{HBs2}}(t_n)$, which shares the same approach with (18), can be given as:

$$\begin{aligned}R_{\mathrm{HBs2}}(t_n)=&\sum_{j_{\mathrm{HB}}=M_{\mathrm{HB}}+1}^{M_{\mathrm{HB}}+M_{\mathrm{UF}}-j_{\mathrm{UF}}+j_{\mathrm{UFp}}}\frac{(N_{\mathrm{HB}}+M_{\mathrm{HB}})!}{j_{\mathrm{HB}}!}(R_{\mathrm{HBn}}(t_n))^{N_{\mathrm{HB}}+M_{\mathrm{HB}}-j_{\mathrm{HB}}}\cdot\\&(1-R_{\mathrm{HBn}}(t_n))^{j_{\mathrm{HB}}}\end{aligned} \tag{21}$$

The reliability of the arm $R_{\mathrm{Arm,u2}}(t_n)$, which shares the same approach with (19), can be given as:

$$R_{\mathrm{Arm,u2}}(t_n)=R_{\mathrm{UFs2}}(t_n)R_{\mathrm{HBs2}}(t_n) \tag{22}$$

Therefore, the overall reliability of the hybrid MMC arm $R_{\mathrm{Arm,u}}(t_n)$ can be obtained by adding (19) and (22) as:

$$R_{\mathrm{Arm,u}}(t_n)=R_{\mathrm{Arm,u1}}(t_n)+R_{\mathrm{Arm,u2}}(t_n) \tag{23}$$

Based on the symmetry of hybrid MMC, the reliability of hybrid MMC $R(t_n)$ can be calculated by:

$$R(t_n)=(R_{\mathrm{Arm,u}}(t_n))^6 \tag{24}$$

The proposed operation strategy considers the SMs with single function status to support the DC-link voltage. In terms of reliability, single-function UFSM which equals to HBSM can increase the number of redundant HBSM. Therefore, the reliability of hybrid MMC can be improved.

V. Experimental Results

In this section, the effectiveness of the proposed operational reliability and operation strategy of hybrid MMC is demonstrated. The Infineon IGBT module FF1000R17IE4 is chosen as the power module in the hybrid MMC [32]. The parameters of the hybrid MMC and WTG are given in Table II. We use the real wind speed and air temperature data of Dublin in Ireland in 2016 [38], which are shown in Fig. 5 and Fig. 6, respectively, and there is 1 s time delay to receive wind among WTGs.

TABLE II
Parameters of Hybrid MMC and WTG

Parameter	Value
System rated active power	312 MW
Rated AC grid voltage	180 kV
Rated DC-link voltage	400 kV
Number of WTG	156
Rated active power of WTG	2 MW
Cut-in wind speed	3 m/s
Rated wind speed	9 m/s
Cut-out wind speed	16 m/s
Number of requisite HBSM	137
Number of requisite UFSM	113
Requisite voltage of capacitor	1.6 kV
Failure rate of capacitor	1×10^{-8}/hour
Fundamental frequency	50 Hz
Switching frequency	1500 Hz
Modulation index	0.9

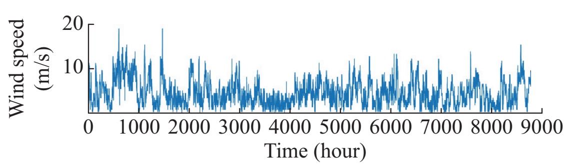

Fig. 5. Wind speed time series.

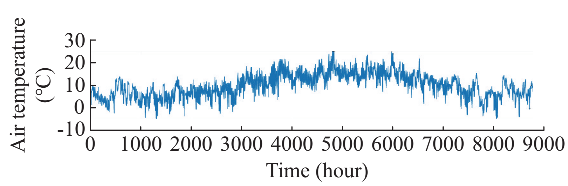

Fig. 6. Air temperature time series.

A. Reliability Differences of Power Devices with Multiple Time Scales

To investigate reliability difference of power devices in different SMs, the consumed lifetimes of power devices with long-term and short-term time scales are obtained and shown in Table III.

As shown in Table III, the long-term thermal cycles, which are caused by wind speed and air temperature, consume more lifetime in T_1, T_2, T_3, D_1 and D_2. However, the short-term thermal cycles, which are caused by electrical factors, cannot be ignored, because their proportions occupy 16.39%, 25.06% and 67.82% of the total consumed lifetime in T_2, D_1 and D_3, respectively. In addition, the short-term thermal cycles of D_3 consume more lifetime than the long-term ones. Consequently, the reliability of power devices in hybrid MMC with multiple time scales is relatively more accurate compared with single time scale, because both environmental and electrical factors have a significant impact on hybrid MMC. Besides, the difference of consumed lifetime among power devices in SM is obvious. For example, in UFSM, T_2 and D_3 consume the most serious lifetime. The same problem occurs in other SMs, e. g., SBSM and CDSM, which are widely used in hybrid MMCs, because they share the similar operation scheme.

B. Reliability of Hybrid MMC with Different SM Operation Strategies

As shown in Table III, the failure probability of module T_3 is higher than other modules in UFSM, as the total consumed lifetime proportion of T_3 and D_3 in UFSM is 50.08%. Therefore, it is worthy to bypass the faulty module T_3 instead of the whole UFSM, when module T_3 fails.

To verify the effectiveness of the proposed strategy, a brief reliability comparison between the conventional strategy and the proposed strategy is carried out. Figure 7 shows the reliability curves R_{chm} and R_{phm} of the conventional strategy and the proposed strategy, respectively, when $M_{UF}=0$, 1, 5, 10 and $M_{HB}=0$. In addition, Table IV shows the operation time with these strategies. In case of $M_{UF}=0$, R_{chm} and R_{phm} have the same reliability level since there is no redundancy to substitute the faulty UFSM and HBSM. In the case of $M_{UF}=5$, both normal and single-function UFSMs can substitute faulty HBSMs, and normal UFSMs can substitute the faulty UFSMs. Compared with R_{chm}, the operation time of R_{phm} increases by 1.5, 1.78, 2.05 and 2.36 years when the reliabilities are 0.8, 0.6, 0.4 and 0.2, respectively.

TABLE III
Consumed Lifetimes of Power Devices in Hybrid MMC

Device	$CL_{\text{long-term}}$		$CL_{\text{short-term}}$		Proportion in HBSM (%)	Proportion in UFSM (%)
	Value	Proportion (%)	Value	Proportion (%)		
T_1	1.09×10^{-5}	91.10	1.06×10^{-6}	8.90	0.93	0.45
T_2	9.27×10^{-4}	83.61	1.89×10^{-4}	16.39	86.55	43.41
T_3	7.97×10^{-6}	99.33	5.36×10^{-8}	0.67	-	0.30
D_1	1.15×10^{-4}	74.94	3.86×10^{-5}	25.06	11.91	5.76
D_2	7.41×10^{-6}	93.98	4.74×10^{-7}	6.02	0.61	0.29
D_3	4.31×10^{-4}	32.18	9.02×10^{-4}	67.82	-	49.78

Note: "-" means the index does not exist.

Therefore, as shown in Table IV, the proposed operation strategy can extend the operation time of UFSM and improve the reliability of hybrid MMC.

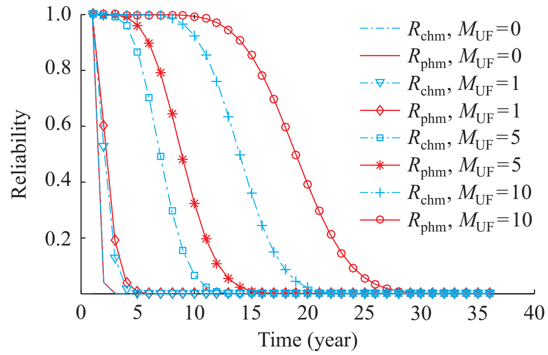

Fig. 7. Reliability of hybrid MMC with different SM operation strategies.

TABLE IV
OPERATION TIME OF HYBRID MMC WITH DIFFERENT SM OPERATION STRATEGIES

Reliability	Operation time (year)							
	$M_{UF}=10$		$M_{UF}=5$		$M_{UF}=1$		$M_{UF}=0$	
	R_{chm}	R_{phm}	R_{chm}	R_{phm}	R_{chm}	R_{phm}	R_{chm}	R_{phm}
0.8	10.63	14.78	4.44	5.94	0.56	0.64	0.07	0.07
0.6	12.27	17.04	5.55	7.28	0.89	1.01	0.17	0.17
0.4	13.72	18.92	6.46	8.51	1.24	1.41	0.30	0.30
0.2	15.43	21.16	7.63	9.99	1.73	1.97	0.52	0.52

C. Operational Reliability of Hybrid MMC

In this subsection, the impact of environmental and electrical factors on the reliability of the developed hybrid MMC model is comprehensively investigated. Hybrid MMC is equipped with requisite HBSM and UFSM in this case.

1) Influence of Wind Speed and Air Temperature

The reliability R_{phm} in the proposed model considering the impact of wind speed and air temperature and R_{chm} in the conventional statistical model are shown in Fig. 8. In addition, the failure rate curves of UFSM and HBSM are shown in Fig. 9. From Fig. 8, it can be observed that the reliability of hybrid MMC varies with the fluctuation of the wind speed and ambient temperature. From 500 hours to 1000 hours, the wind speed is continuous at a high level (from 7 m/s to 10 m/s as shown in Fig. 5). Accordingly, the failure rates of UFSM and HBSM are concentrated on 0.9×10^{-6} per hour and 1.8×10^{-6} per hour, respectively. Therefore, the reliability of hybrid MMC R_{phm} decreases rapidly. On the contrary, from 3500 hours to 4000 hours, under the condition of low wind speed ranging from 1 m/s to 4 m/s, both UFSM and HBSM keep in low failure rates. Consequently, the reliability of hybrid MMC R_{phm} worsens slowly in Fig. 8. Similarly, from 4000 hours to 6000 hours, under the condition of relatively higher air temperature, hybrid MMC suffers from more serious thermal fatigue. Therefore, the failure rates of UFSM and HBSM are relatively higher as shown in Fig. 9. All above, the proposed reliability model is consistent with the theoretical expectation. In general, the R_{chm} obtained by classical model neglects the impact of environmental factors, hence, the deviations between the conventional and the proposed operational reliability at 1000 hours, 4000 hours and 7000 hours are as high as 41.38%, 34.45% and 82.36%, respectively. Therefore, it is worthy to consider the impact of environmental factors on the operational reliability of hybrid MMC.

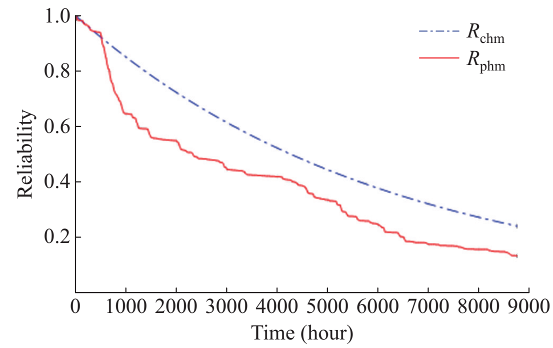

Fig. 8. Reliability of hybrid MMC affected by wind speed and air temperature.

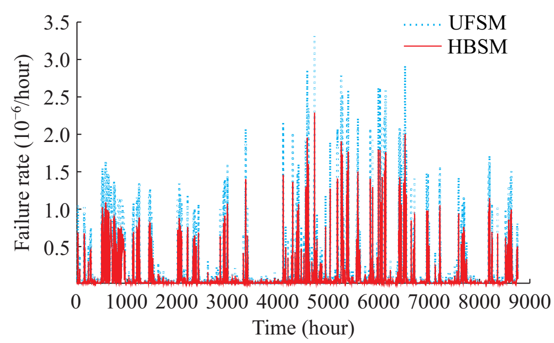

Fig. 9. Failure rate of UFSM and HBSM affected by wind speed and air temperature.

2) Influence of Switching Frequency

Based on the proposed model, the reliability curves with different switching frequencies are obtained in Fig. 10. Table V shows the reliability indices of hybrid MMC with different switching frequencies at 900 hours.

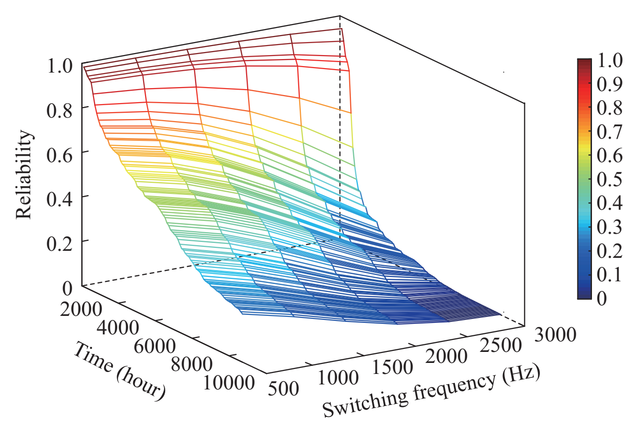

Fig. 10. Reliability of hybrid MMC with different switching frequencies.

As shown in Fig. 10, when the switching frequency is

TABLE V
RELIABILITY INDICES OF HYBRID MMC AT 900 HOURS

Switching frequency (Hz)	Reliability	Failure rate of UFSM per hour	Failure rate of HBSM per hour
1000	0.7150	6.91×10^{-7}	1.56×10^{-7}
2000	0.5426	1.09×10^{-6}	5.54×10^{-7}
3000	0.2572	2.17×10^{-6}	1.63×10^{-6}

high, the reliability of hybrid MMC decreases rapidly. For instance, at 900 hours, when the switching frequency increases from 1000 Hz to 3000 Hz, the power devices in hybrid MMC suffer from more switching losses. This causes the failure rate of UFSM to increase from 6.91×10^{-7} per hour to 2.17×10^{-6} per hour, and the failure rate of HBSM increases from 1.56×10^{-7} per hour to 1.63×10^{-6} per hour. Furthermore, the reliability of hybrid MMC decreases from 0.715 to 0.257 (decreases by 178.21%). Hence, the switching frequency has a significant effect on the reliability of hybrid MMC. The R_{chm} obtained by classical model neglects the impact of electrical factors as shown in Fig. 8. Compared with the proposed operational reliability of hybrid MMC with 1000 Hz, 2000 Hz and 3000 Hz, the classical reliability deviations are as high as 14.92%, 59.27% and 229% at 900 hours, respectively. Therefore, it is worthy to consider the impact of electrical factors.

VI. CONCLUSION

This paper proposes an operational reliability model of hybrid MMC considering multiple time scales and multi-state SM, for wind power transmission application. The main advantages of the proposed operational reliability model can be summarized as follows.

1) We find that the reliability differences among power devices in hybrid MMC are obvious for wind power transmission. In the same module, T_2 and D_3 suffer most serious stress. It provides a guidance to improve the reliability of hybrid MMC such as decreasing the switching frequency.

2) In terms of reliability, the proposed operation strategy considering multi-state SM can be used to extend the operation time of SM and improve the reliability of hybrid MMC effectively.

3) The proposed operational reliability model of hybrid MMC can effectively characterize the impact of environmental and electrical factors compared with the conventional model.

These advantages have been verified by using the obtained results.

REFERENCE

[1] J. Lyu, X. Cai, and M. Molinas, “Optimal design of controller parameters for improving the stability of MMC-HVDC for wind farm integration,” *IEEE Journal of Emerging and Selected Topics in Power Electronics*, vol. 6, no. 1, pp. 40-53, Mar. 2018.
[2] S. Debnath, J. Qin, B. Bahrani *et al*., “Operation, control, and applications of the modular multilevel converter: a review,” *IEEE Transactions on Power Electronics*, vol. 30, no. 1, pp. 37-53, Jan. 2015.
[3] M. A. Perez, S. Bernet, J. Rodriguez *et al*., “Circuit topologies, modeling, control schemes, and applications of modular multilevel converters,” *IEEE Transactions on Power Electronics*, vol. 30, no. 1, pp. 4-17, Jan. 2015.
[4] A. Isidori, F. M. Rossi, F. Blaabjerg *et al*., “Thermal loading and reliability of 10-MW multilevel wind power converter at different wind roughness classes,” *IEEE Transactions on Industry Applications*, vol. 50, no. 1, pp. 484-494, Jan.-Feb. 2014.
[5] R. O. Sousa, J. V. M. Farias, A. F. Cupertino *et al*., “Life consumption of an MMC-STATCOM supporting wind power plants: impact of the modulation strategies,” *Microelectronics Reliability*, vol. 88-90, pp. 1063-1070, Sept. 2018.
[6] H. Liu, K. Ma, Z. Qin *et al*., “Lifetime estimation of MMC for offshore wind power HVDC application,” *IEEE Journal of Emerging and Selected Topics in Power Electronics*, vol. 4, no. 2, pp. 504-511, Jun. 2016.
[7] L. Wang, J. Xu, G. Wang *et al*., “Lifetime estimation of IGBT modules for MMC-HVDC application,” *Microelectronics Reliability*, vol. 82, pp. 90-99, Mar. 2018.
[8] K. Ma, M. Liserre, F. Blaabjerg *et al*., “Thermal loading and lifetime estimation for power device considering mission profiles in wind power converter,” *IEEE Transactions on Power Electronics*, vol. 30, no. 2, pp. 590-602, Feb. 2015.
[9] R. Zeng, L. Xu, L. Yao *et al*., “Design and operation of a hybrid modular multilevel converter,” *IEEE Transactions on Power Electronics*, vol. 30, no. 3, pp. 1137-1146, Mar. 2015.
[10] R. Zeng, L. Xu, L. Yao *et al*., “Precharging and DC fault ride-through of hybrid MMC-based HVDC systems,” *IEEE Transactions on Power Delivery*, vol. 30, no. 3, pp. 1298-1306, Jun. 2015.
[11] J. Xu, P. Zhao, and C. Zhao, “Reliability analysis and redundancy configuration of MMC with hybrid submodule topologies,” *IEEE Transactions on Power Electronics*, vol. 31, no. 4, pp. 2720-2729, Apr. 2016.
[12] J. Guo, X. Wang, J. Liang *et al*., “Reliability modelling and evaluation of MMCs under different redundancy schemes,” *IEEE Transactions on Power Delivery*, vol. 33, no. 5, 2087-2096, Oct. 2017.
[13] P. Tu, S. Yang, and P. Wang, “Reliability- and cost-based redundancy design for modular multilevel converter,” *IEEE Transactions on Industrial Electronics*, vol. 66, no. 3, pp. 2333-2342, Mar. 2019.
[14] B. Wang, X. Wang, Z. Bie *et al*., “Reliability model of MMC considering periodic preventive maintenance,” *IEEE Transactions on Power Delivery*, vol. 32, no. 3, pp. 1535-1544, Jun. 2017.
[15] J. Guo, J. Liang, X. Zhang *et al*., “Reliability analysis of MMCs considering submodule designs with individual or series-operated IGBTs,” *IEEE Transactions on Power Delivery*, vol. 32, no. 2, pp. 666-677, Apr. 2017.
[16] H. Li, M. Zheng, R. Yao *et al*., “Reliability modelling and analysis on MMC for VSC-HVDC by considering the press-pack IGBT and capacitors failure,” *The Journal of Engineering*, vol. 2019, no. 16, pp. 2219-2223, Apr. 2019.
[17] J. Xu, H. Jing, and C. Zhao, “Reliability modeling of MMCs considering correlations of the requisite and redundant submodules,” *IEEE Transactions on Power Delivery*, vol. 33, no. 3, pp. 1213-1222, Jun. 2018.
[18] J. Xu, L. Wang, D. Wu *et al*., “Reliability modeling and redundancy design of hybrid MMC considering decoupled sub-module correlation,” *International Journal of Electrical Power & Energy Systems*, vol. 105, pp. 690-698, Feb. 2019.
[19] J. Xu, L. Wang, Y. Li *et al*., “A unified MMC reliability evaluation based on physics-of-failure and SM lifetime correlation,” *International Journal of Electrical Power & Energy Systems*, vol. 106, pp. 158-168, Mar. 2019.
[20] H. Wang, M. Liserre, F. Blaabjerg *et al*., “Transitioning to physics-of-failure as a reliability driver in power electronics,” *IEEE Journal of Emerging and Selected Topics in Power Electronics*, vol. 2, no. 1, pp. 97-114, Mar. 2014.
[21] M. Pecht and J. Gu. “Physics-of-failure-based prognostics for electronic products,” *Transactions of the Institute of Measurement and Control*, vol. 31, pp. 309-322, Jun. 2009.
[22] K. C. Norris and A. H. Landzberg, “Reliability of controlled collapse interconnections,” *IBM Journal of Research and Development*, vol. 13, no. 3, pp. 266-271, May 1969.
[23] R. Bayerer, T. Herrmann, T. Licht *et al*., “Model for power cycling lifetime of IGBT modules – various factors influencing lifetime,” in *Proceedings of 5th International Conference on Integrated Power Electronics Systems*, Nuremberg, Germany, Mar. 2008, pp. 1-6.
[24] X. Du, G. Li, T. Li *et al*., “Multi-time scale lifetime evaluation of IGBT modules in the wind power converter,” *Proceedings of the CSEE*, vol. 35, no. 29, pp. 6152-6161, Dec. 2019.
[25] H. Huang and P. A. Mawby, “A lifetime estimation technique for voltage source inverters,” *IEEE Transactions on Power Electronics*, vol.

28, no. 8, pp. 4113-4119, Aug. 2013.

[26] M. A. Miner, "Cumulative damage in fatigue," *Journal of Applied Mechanics*, vol. 12, no. 3, pp. A159-A164, Sept. 1945.

[27] J. Qin, M. Saeedifard, A. Rockhill *et al*., "Hybrid design of modular multilevel converters for HVDC systems based on various submodule circuits," *IEEE Transactions on Power Delivery*, vol. 30, no. 1, pp. 385-394, Feb. 2015.

[28] W. Xiang, W. Lin, J. Wen *et al*., "A new topology of sub-modules with DC fault current blocking capability and a new type of hybrid MMC converter," *Proceedings of the CSEE*, vol. 34, no. 29, pp. 5171-5179, Oct. 2014.

[29] S. H. Jangamshetti and V. G. Rau, "Site matching of wind turbine generators: a case study," *IEEE Transactions on Energy Conversion*, vol. 14, no. 4, pp. 1537-1543, Dec. 1999.

[30] T. Lei, M. Barnes, and A. C. Smith, "Thermal cycling evaluation for DFIG wind turbine power converter based on joint modelling," in *Proceedings of 2013 IEEE Energy Conversion Congress and Exposition*, Denver, USA, Sept. 2013, pp. 3845-3851.

[31] G. Li, X. Du, P. Sun *et al*., "Numerical IGBT junction temperature calculation method for lifetime estimation of power semiconductors in the wind power converters," in *Proceedings of 2014 International Power Electronics and Application Conference and Exposition*, Shanghai, China, Nov. 2014, pp. 49-55.

[32] L. Wei, R. J. Kerkman, R. A. Lukaszewski *et al*., "Analysis of IGBT power cycling capabilities used in doubly fed induction generator wind power system," *IEEE Transactions on Industry Applications*, vol. 47, no. 4, pp. 1794-1801, Jul.-Aug. 2011.

[33] Infineon Technologies AG. Infineon IGBT module datasheet (FF1000R17IE4). [Online]. Available: http://www.infineon.com

[34] M. Matsuishi and T. Endo. (1968, Jan.). Fatigue of metals subjected to varying stress. [Online]. Available: https://scinapse.io/papers/37625411

[35] L. Wei, R. J. Kerkman, and R. A. Lukaszewski, "Evaluation of power semiconductors power cycling capabilities for adjustable speed drive," in *Proceedings of 2008 IEEE Industry Applications Society Annual Meeting*, Edmonton, Canada, Oct. 2008, pp. 1-10.

[36] D. Hirschmann, D. Tissen, S. Schroder *et al*., "Reliability prediction for inverters in hybrid electrical vehicles," *IEEE Transactions on Power Electronics*, vol. 22, no. 6, pp. 2511-2517, Nov. 2007.

[37] Y. Chen, H. Li, F. Lin *et al*., "Study on self-healing and lifetime characteristics of metallized-film capacitor under high electric field," *IEEE Transactions on Plasma Science*, vol. 40, no. 8, pp. 2014-2019, Aug. 2012.

[38] Case data. [Online]. Available: https://www. figshare. com/articles/Test-Data/8230766

Fei Feng is pursuing the master degree in the School of Electrical Engineering, Chongqing University, Chongqing, China. His research interests include operation reliability assessment in power and electrical system.

Juan Yu received the Ph.D. degree in electrical engineering from Chongqing University, Chongqing, China, in 2007. She is now a Full Professor with the School of Electrical Engineering, Chongqing University. Her research interests include big data application, optimal reactive power flow and risk assessment in power systems.

Wei Dai received the Ph.D. degree from School of Electrical Engineering, Chongqing University, Chongqing, China, in 2018. His research interests include power system analysis and large-scale system problems.

Zhifang Yang received the Ph.D. degree in electrical engineering from Tsinghua University, Beijing, China, in 2018. He is now an Assistant Professor with the School of Electrical Engineering, Chongqing University, Chongqing, China. His research interests include power system analysis and electricity market.

Xingpan Zhao received the master degree in the School of Electrical Engineering, Chongqing University, Chongqing, China. He is now an Engineer with the Chuxiong Power Supply Bureau of Yunnan Power Grid, Chuxiong, China. His research interest includes converter maintenance.

Salah Kamel received the international Ph. D. degree from University of Jaen, Jaen, Spain (Main) and Aalborg University, Aalborg, Denmark (Host). He is currently a Senior Research Fellow in State Key Laboratory of Power Transmission Equipment & System Security and New Technology, School of Electrical Engineering, Chongqing University, Chongqing, China. His research interests include power system modeling, analysis and optimization, renewable energy and smart grid technologies.

Guobin Fu is currently an Assistant Engineer with the Electric Power Research Institute, State Grid Qinghai Electric Power Company, Xining, China. His research interests include network-related safety testing and debugging of grid-connected units.